

HYDRODYNAMIC SIMULATIONS OF THE SUNYAEV-ZEL'DOVICH EFFECT(S)

VOLKER SPRINGEL, MARTIN WHITE, AND LARS HERNQUIST

Harvard-Smithsonian Center for Astrophysics, Cambridge, MA 02138

Draft version October 24, 2018

ABSTRACT

We have performed a sequence of high resolution hydrodynamic simulations of structure formation in a Λ CDM model to study the thermal and kinetic Sunyaev-Zel'dovich (SZ) effects. Including only adiabatic gas physics, we demonstrate that our simulations for the thermal effect are converged down to sub-arcminute scales. In this model, the angular power spectrum of CMB anisotropies induced by the thermal effect peaks at $\ell \simeq 10^4$, and reaches an amplitude just below current observational upper limits. Fluctuations due to the kinetic effect are a factor of $\simeq 30$ lower in power and peak at slightly smaller angular scales. We identify individual SZ sources and compute their counts as a function of source strength and angular size. We present a preliminary investigation of the consequences of an early epoch of energy injection which tends to suppress power on small angular scales, while giving rise to additional power on large scales from the reheated IGM at high redshift.

Subject headings: cosmic microwave background – cosmology: theory – galaxies: clusters: general – large-scale structure of universe – methods: numerical

1. INTRODUCTION

On angular scales below $10'$, the microwave sky carries the imprint of large-scale structure in the low- z universe. In particular, cosmic microwave background (CMB) photons propagating through the universe are inverse Compton or Doppler scattered by hot electrons along their path, either in dense structures such as clusters of galaxies or more generally in hot gas in the intergalactic medium. Inverse Compton scattering conserves the number of photons but preferentially increases their energy, leading to a spectral distortion whose amplitude is proportional to the product of the electron temperature and density (or pressure). Doppler scattering induces an intensity fluctuation with the same spectral shape as the CMB itself. These effects were first described by Sunyaev & Zel'dovich (1972, 1980) and are known as the thermal and kinetic SZ effects, respectively (for recent reviews see Rephaeli 1995 and Birkinshaw 1999).

The thermal effect is one of the primary sources of secondary anisotropies in the CMB on small angular scales. The change in the (thermodynamic) temperature of the CMB resulting from scattering off non-relativistic electrons is

$$\frac{\Delta T}{T} = y \left(x \frac{e^x + 1}{e^x - 1} - 4 \right) \quad (1)$$

$$\simeq -2y \quad \text{for } x \ll 1, \quad (2)$$

where $x = h\nu/kT_{\text{CMB}} \simeq \nu/56.85$ GHz is the dimensionless frequency, and the second expression is valid in the Rayleigh-Jeans limit which we shall assume henceforth. The quantity y is known as the Comptonization parameter and is given by

$$y \equiv \sigma_T \int dl \frac{n_e k(T_e - T_{\text{CMB}})}{m_e c^2}, \quad (3)$$

where the integral is performed along the photon path. Since $T_e \gg T_{\text{CMB}}$ the integrand is proportional to the integrated electron pressure along the line of sight.

The kinetic SZ effect arises from the motion of ionized gas with respect to the rest-frame of the CMB. The resulting temperature fluctuation is $\Delta T/T = -b$, where

$$b \equiv \sigma_T \int dl n_e \frac{v_r}{c} \quad (4)$$

measures the magnitude of the effect along the line of sight if v_r is the radial peculiar velocity of the gas. The different dependence on frequency of the two effects can, in principle, be used to disentangle them observationally, though the primary CMB anisotropies provide “noise” for the kinetic SZ signal. The imprint of the SZ effects on the CMB has been studied by a number of authors (Ostriker & Vishniac 1986, Persi et al. 1995, da Silva et al. 2000, Refregier et al. 2000, Seljak et al. 2000, among others), but the theoretical predictions still exhibit substantial quantitative uncertainty.

In this paper, we report first results of a sequence of high resolution hydrodynamic simulations designed to study the SZ signal on small angular scales. Our simulations can be used to calibrate and test the semi-analytic modelling that has been done before, explore the effect of varying the physics included, and provide predictions for upcoming experiments. In Section 2, we describe our simulation set and we discuss the techniques we use to compute SZ maps. In Section 3, we present our results for the power spectra of thermal and kinetic SZ effects, and we show SZ source counts as a function of source strength and source size. Finally, we summarize and discuss our results in Section 4.

2. METHOD

We are interested primarily in the consequences of assumptions about the physical state of the gas for predictions of the SZ signal, so we have focussed on one particular cosmological model, chosen from the Λ CDM family. For definiteness, we have adopted the “concordance” model of Ostriker & Steinhardt (1995) which has $\Omega_m = 0.3$, $\Omega_\Lambda = 0.7$, $H_0 = 100 h \text{ km s}^{-1} \text{ Mpc}^{-1}$ with

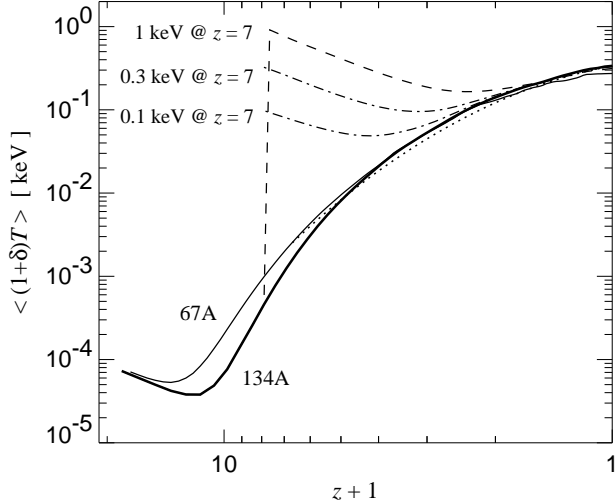


FIG. 1.— The evolution of the density weighted temperature with redshift. The solid and dashed lines are the simulation results, while the dotted line shows our predictions based on the Press-Schechter theory.

$h = 0.67$, $\Omega_B = 0.04$, $n = 1$ and $\sigma_8 = 0.9$ (corresponding to $\delta_H = 5.02 \times 10^{-5}$). This model yields a reasonable fit to the current suite of cosmological constraints and as such provides a good framework for making realistic predictions.

We ran a number of simulations on the Cray T3E at the San Diego Supercomputing Center using the GADGET Tree/SPH code (Springel, Yoshida & White 2000). Each simulation employed 2×224^3 particles and was carried out on 64 processors. Our basic model had a box size of $134 h^{-1} \text{Mpc}$, so the dark matter particles had masses of $1.5 \times 10^{10} h^{-1} M_\odot$ and the SPH particles $2.4 \times 10^9 h^{-1} M_\odot$. The SPH densities were computed from 32 neighbours, so our minimum gas resolution was roughly $8 \times 10^{10} h^{-1} M_\odot$. Our base simulation (134A) was evolved from $z = 50$ to $z = 0$, and the gravitational force softening was of a spline form (e.g. Hernquist & Katz 1989), with a Plummer-equivalent softening length of $25 h^{-1} \text{kpc}$ comoving.

As a test of our numerical resolution we also simulated the same cosmological model in a $67 h^{-1} \text{Mpc}$ box (evolved from $z = 100$ to the present; 67A), with a softening length half that of the 134A run and eight times better mass resolution. In all our runs, the full simulation box was output at 333 different times, between redshifts $z \simeq 19$ and $z = 0$. The simulations reported here followed only adiabatic gas physics. Since the SZ effect is dominated by massive objects with large cooling times this is a reasonable first approximation.

To investigate the effect of an early epoch of energy injection we took the $z = 7$ output of 134A and added 0.1 keV, 0.3 keV or 1 keV of energy per (gas) particle. This injection scenario was deliberately chosen to be somewhat artificial. A more realistic approach might be to add the energy only to gas within halos above a certain density, to describe energy input from galaxy winds or QSO activity for example, or to add it over an extended period of time. Unfortunately, the very large parameter space of these possibilities cannot be explored easily. We thus decided to examine an “extreme” scenario to get a handle on the dependence of the small angle SZ signal on the amount of energy

injected. The amount of extra energy was chosen to be plausible given the observed luminosity–temperature relation in clusters of galaxies (Cavaliere, Menci & Tozzi 1998; Wu, Fabian & Nulsen 1998) and the expected X-ray background from the diffuse intergalactic medium (Pen 1999). We added the energy at $z = 7$, which we also took to be the epoch of reionization, so that the energy injection takes place “before” the gas contributes significantly to the SZ signal. A visual inspection of slices through the simulation shows that an energy injection as large as 1 keV literally blows gas out of small halos, leaving only the gas in the larger collapsed objects. The gas is thus more smoothly distributed in addition to being hotter. At $z = 0$ the slope of the mass weighted temperature–mass relation in the 1 keV simulation is thus changed from a canonical 1.5 to a considerably steeper 1.7.

The evolution of the density weighted temperature in our simulations is shown in Fig. 1. Note the good convergence between the large (134A) and the small box (67A) at redshifts $z < 5$. In the 67A run, the adiabatic decay of the mean temperature is halted at a somewhat higher redshift, as expected: due to the better mass resolution of this simulation, nonlinear structures of small mass collapsing at earlier times can be resolved. In the runs with energy injection, the temperature increases discontinuously at $z = 7$, and then declines again with the adiabatic expansion, until shock heating takes over at $z \sim 1 - 3$, depending on the amount of injected energy. At $z = 0$, all runs yield a mean mass-weighted temperature of $\simeq 0.3 \text{ keV}$.

We produced maps in a manner similar to da Silva et al. (2000). First, the various outputs from the boxes were “stacked” back along the line of sight, with each box randomly translated and oriented in the direction of either the x , y or z axis. Then, a grid of 512^2 rays subtending a constant angle of 1° from the observer was traced through the boxes starting at $z = 19$. For our choice of an opening angle of 1° , the full $134 h^{-1} \text{Mpc}$ box just subtends an angle equal to the field of view at $z = 19$. For the smaller $67 h^{-1} \text{Mpc}$ run, the field of view reaches the box size at a distance $z \simeq 2$, beyond which we covered it by periodic replication of the box.

We produced maps of the y -parameter, the Doppler b -parameter, and the projected gas and dark matter densities. For example, the y temperature decrement along any ray was calculated by distributing the product of pressure and specific volume of the gas particles over the angular grid:

$$y_{ij} L_{\text{pix}}^2 = \frac{\sigma_T}{m_e c^2} \sum_{\alpha} p_{\alpha} w_{\alpha, ij}, \quad (5)$$

where $w_{\alpha, ij}$ is the value of the (projected) smoothing kernel (normalized to unity for the pixels covered) of particle α at angular grid position (ij) , and L_{pix}^2 is the physical area of a pixel at the particle’s distance.

The product of pressure and volume, p_{α} , for each SPH particle is

$$p = (\gamma - 1)(1 - Y_p) m u \mu x_e, \quad (6)$$

where γ is the ratio of specific heats, $Y_p = 0.24$ the primordial ^4He mass fraction, m the particle mass, u the internal energy per unit mass, μ the mean molecular weight and x_e the ratio of electron and hydrogen number densities. In the runs reported here, we do not track x_e dynamically. Instead, we set it to 1.158 for temperatures above

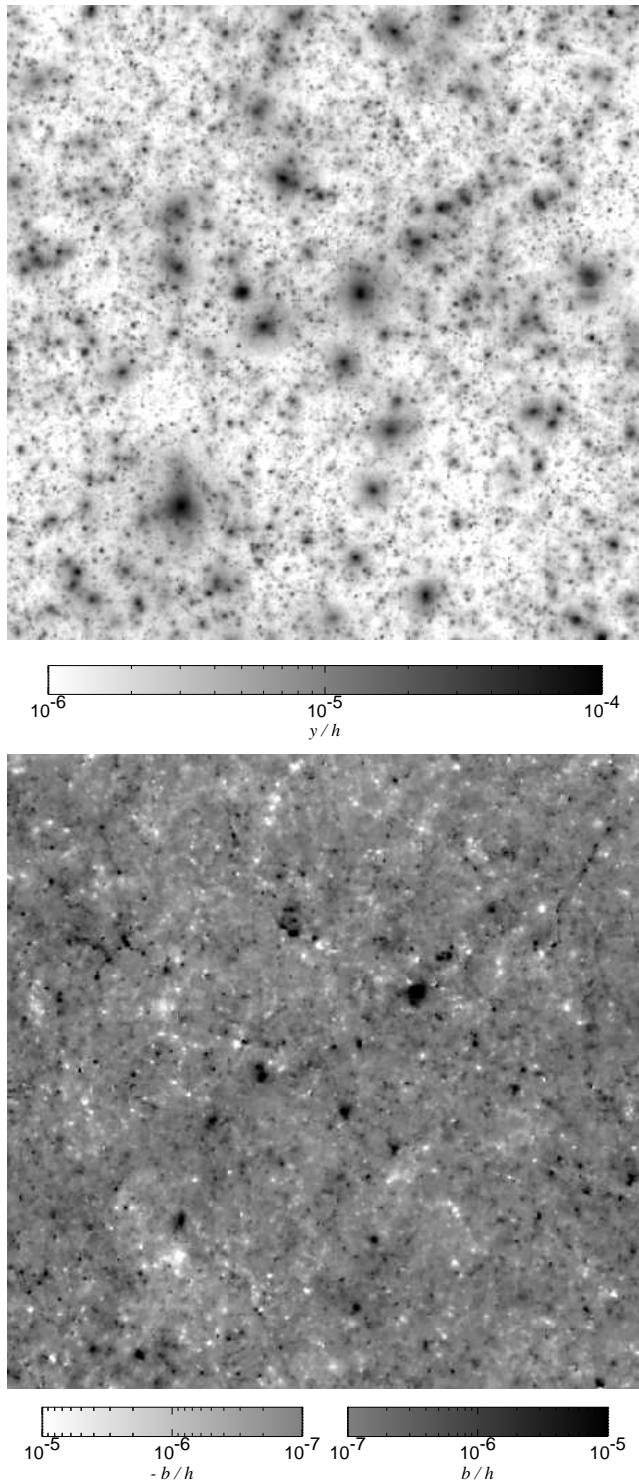


FIG. 2.— Maps of the thermal (top) and kinetic (bottom) SZ effects. The maps are 1° on a side and cover both the same field of view, here computed for the 134A simulation. Notice that unlike the Comptonization y , the kinetic signal b may be negative; we map the negative values onto the lower half of a logarithmic grayscale. Structures appearing in white are moving towards the observer, those in black away.

10^4 K, corresponding to full ionization, and take the gas at lower temperature to be neutral. In reality, the inclusion of an ionizing background would render this assumption invalid at low redshift, but the small densities of the af-

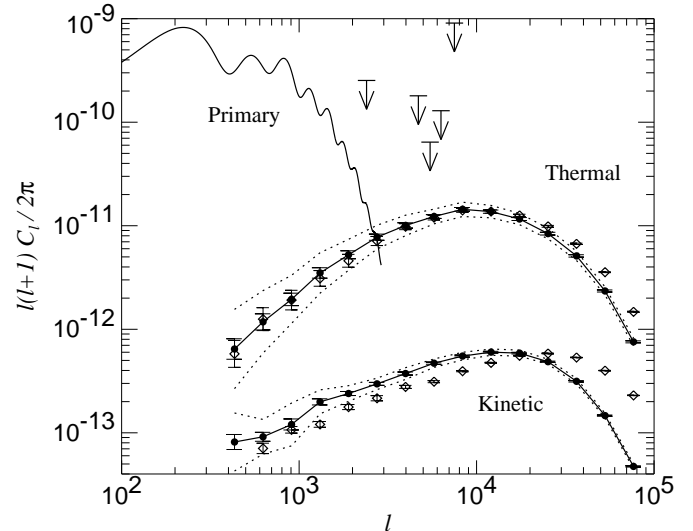


FIG. 3.— The angular power spectrum of the SZ effect from an ensemble of 15 maps. The upper solid line shows the primary CMB anisotropies for this model. The points indicate the mean and error on the mean from our ensemble of maps. Filled circles mark results for the 134A simulation, open diamonds are for the smaller 67A-box. The dotted lines indicate the field-to-field variance between individual 1° maps. The arrows at upper right are 95% CL upper limits from a variety of experiments: SUZIE (Church et al. 1997), ATCA (Subrahmanyam et al. 1993, 1998), BIMA (Holzapfel et al. 2000), Ryle (Jones 1997), and VLA (Partridge et al. 1997).

fected gas do not lead to any significant contribution to the SZ signals. These are thus unaffected by our assumption about the ionization state of the gas, provided ionization happens late enough. On the other hand, it is crucial to assume that the gas is neutral at very high redshift, otherwise the high physical density of the ambient gas in this regime would give rise to a significant contribution to the SZ effects. In particular, the finite box size of our simulations would then lead to a strong signal for the kinetic effect on large angular scales, reflecting motion of gas due to the largest modes in the box.

3. RESULTS

We show typical examples for our thermal and kinetic SZ maps in Fig. 2. These maps were produced by coadding a large number of partial maps, each giving the contribution of one of the boxes that we stacked along the photon's path. It is interesting to note that filamentary structure is easily detected in these partial maps with their small depth in redshift space. However, in the full projection along the backward photon path, filaments are largely hidden in the high level of background arising from the summation over many of these structures. Things may not be quite so bad for the kinetic effect, where it seems that a somewhat larger degree of filamentary structure manages to survive at appreciable signal. Note that sources that are “bright” in the thermal effect are not necessarily among the brightest in the kinetic effect, and vice versa. Often, the kinetic effect shows neighboring large peaks of opposite sign. This may be useful in strategies for identifying clusters and superclusters (Diaferio, Sunyaev & Nusser 2000).

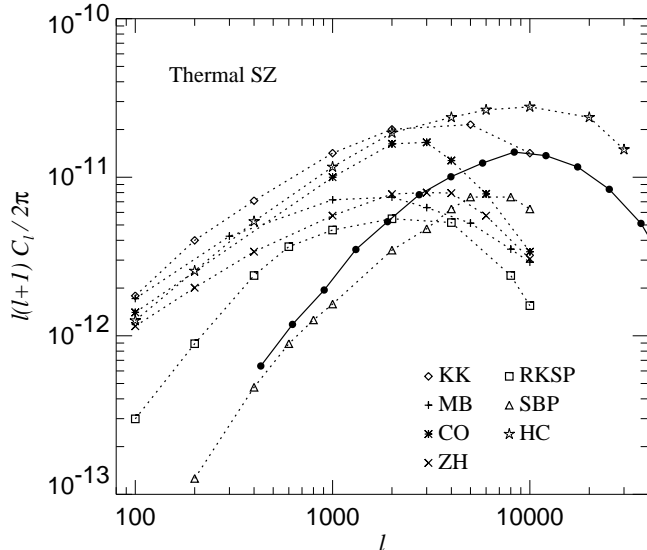


FIG. 4.— Published estimates of the thermal SZ power spectrum compared to the result of this work. Filled circles show our measurement, while other symbols give computations by the following authors: KK (Komatsu & Kitayama 1999), MB (Molnar & Birkinshaw 2000), CO (Cooray 2000), ZH (Zhang & Pen 2000), RKSP (Refregier et al. 2000), SBP (Seljak et al. 2000), and HC (Holder & Carlstrom 1999).

3.1. Power spectra

For each map we computed a number of statistics, and we in general averaged the results for 15 random lines of sight to reduce field-to-field variance. Of most interest here are the angular power spectrum of the thermal and kinetic SZ effects (Fig. 3).

A comparison of our basic $67 h^{-1}$ Mpc and $134 h^{-1}$ Mpc runs shows that for the physics we have included we have converged in the mean mass-weighted temperature and the angular power spectrum for $\ell \leq 20000$, albeit some small residual resolution effects are visible for the kinetic effect. The good level of agreement for the two different runs down to very small angular scales builds confidence in our numerical technique. While this is to be expected as the signal is dominated by structures of mass $> 10^{13} M_{\odot}$, which should be well covered by our resolution, it also suggests that finite box size and the box stacking technique (White & Hu 2000) are not a source of significant uncertainty in our results.

We note that the small box gives slightly more power at $\ell \gtrsim 20000$ for the thermal effect, indicating its better resolution, while at lower ℓ the convergence is excellent. This is also reflected in the mean Comptonization, which both models give as $\langle y \rangle = 2.6 \times 10^{-6}$. For the kinetic effect, we observe a higher level of additional small-scale power for the small box on one hand, and slightly less power for all ℓ below $\ell \simeq 20000$ on the other hand. This suppression likely originates from a deficit of large-scale power in the small box, which reduces the amplitude of peculiar velocities.

Interestingly, the power spectrum of the thermal SZ effect is not far from current observational upper limits, making it a highly interesting target for upcoming experiments. The power in fluctuations due to the kinetic SZ effect is substantially smaller, but may not be out of reach

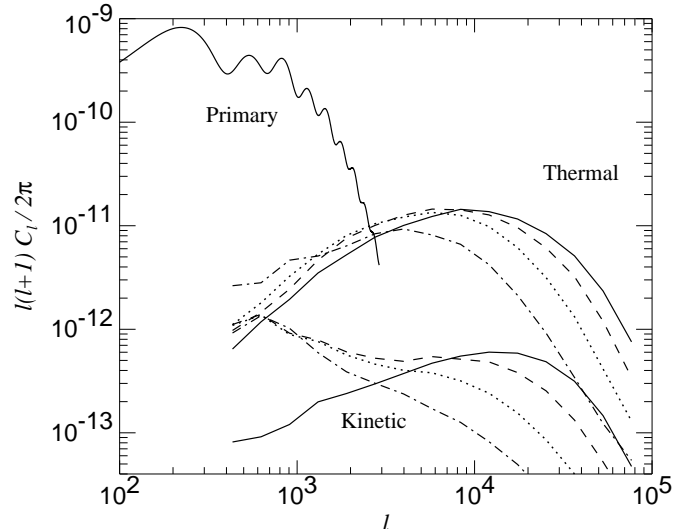


FIG. 5.— Energy injection and its impact on the angular power spectrum of the SZ effect. The upper solid line shows the primary CMB anisotropies for this model, and the lower solid lines give the secondary anisotropies for thermal and kinetic SZ effects in our 134A simulation. Dashed, dotted, and dot-dashed lines show the effect of an injection of 0.1, 0.3, and 1.0 keV of energy at $z = 7$, respectively. Results are based on ensembles of 15 maps for each of our numerical simulations.

in future experiments, especially when multi-frequency observations are employed.

It is interesting to compare published results for the power spectrum of the thermal SZ effect with our measurement, as we have done in Figure 4. There are order of magnitude differences between the various results. Note that slight differences in the adopted cosmological models can partly account for these discrepancies, but even for cosmological parameters that are very close, substantial uncertainties remain. One group of results in this comparison is based on analytical computations, using either extensions of Press-Schechter theory (Komatsu & Kitayama 1999, Holder & Carlstrom 1999, Cooray 2000, Molnar & Birkinshaw 2000) or non-linear perturbation theory (Zhang & Pen 2000). Compared to our result, these computations suggest more power on large angular scales, and their spectrum usually peaks at somewhat larger angular scale, corresponding to ℓ of a few thousand. On the other hand, the numerical work by Seljak et al. (2000), which is based on simulations using a moving-mesh hydrodynamical code (Pen 1998), suggests a very similar shape for the spectrum, but with an amplitude which is a factor 1.5-2 lower than our result. Refregier et al. (2000) use the same simulation technique as Seljak et al. (2000), albeit at lower resolution and in combination with a different analysis of the simulation outputs. Their spectrum peaks at an angular scale of $\ell \simeq 2000$, roughly at the upper boundary of the author's own range of confidence of $200 < \ell < 2000$ for their result.

In general, predictions in the literature for the kinetic SZ effect show a similar degree of quantitative uncertainty. Note however that the computations by Bruscoli et al. (1999) are very close to our result, as is Hu & White (1996) if reionization is assumed to happen late. On the other hand, the signals computed for inhomogeneous reioniza-

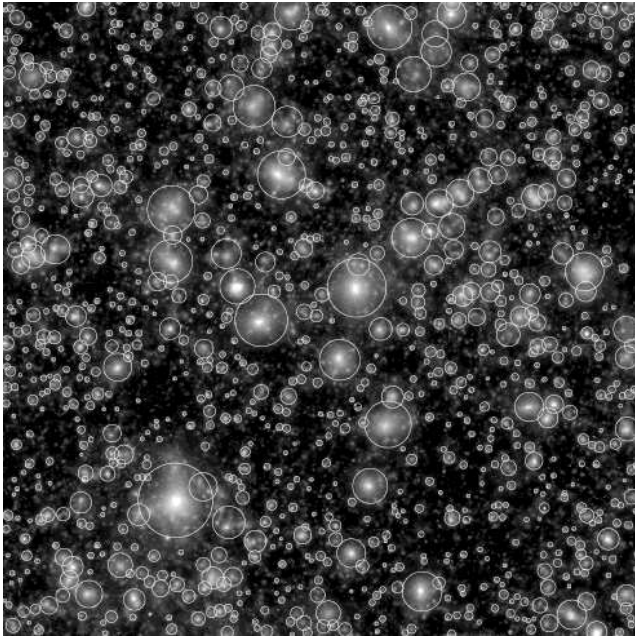


FIG. 6.— Thermal SZ sources identified with SExtractor. A circle is drawn for each source, with area equal to the area determined by the source detection software. The map shown in this example is the same as in Fig. 2, but here displayed with reversed video for graphical clarity.

tion (Gruzinov & Hu 1998, Benson et al. 2000, Valageas et al. 2000) are typically an order of magnitude smaller in power at the peak of the spectrum.

The relatively large scatter in these computations highlights that there is still substantial quantitative uncertainty in the theoretical predictions for the SZ power spectrum. High-resolution simulations like the ones discussed here should help to lead to a more reliable answer.

An additional complication besides computational uncertainties is that the theoretical predictions depend quite sensitively on the physics of reionization and preheating, especially for scales $\ell \gtrsim 2000$, where the SZ effect dominates over primary CMB fluctuations. This is seen when analyzing the SZ signals of our energy injection runs (Fig. 5). Depending on the amount of energy injected, fluctuations on small angular scales can be suppressed very strongly, while additional power on large scales is seen from relatively diffuse, ionized gas. This signal on large angular scales is generated in a small redshift range right after the energy has been injected. Note that on the largest scales we probe, the amplitude of the kinetic SZ effect then becomes dominated by finite box size effects as the signal reflects the largest modes that are present in the simulation.

Apart from influencing the power spectrum, energy injection also alters the mean Comptonization of the models. It becomes $\langle y \rangle = 6.9 \times 10^{-6}$ for the 0.1 keV model, 16.6×10^{-6} for the 0.3 keV run, and reaches 38.0×10^{-6} for an injection of 1 keV. The latter is thus strongly excluded by the upper limit of 15×10^{-6} from the COBE FIRAS experiment (Fixsen et al. 1996), and even the 0.3 keV model is marginally excluded. This highlights the power of the FIRAS constraint.

3.2. Source counts

The maps for the thermal SZ effect are dominated by discrete sources, as suggested by visual inspection. We have used the source detection software SExtractor (Bertin & Arnouts 1996) to count individual sources, and to measure their strength. A similar technique has been employed by da Silva et al. (2000). Figure 6 shows a typical source detection, here obtained for the map shown in Fig 2. To mark each source, we have drawn a circle with area equal to the area of the ellipse matched by SExtractor to each source. We used default settings for the detection algorithm of the image processing software and let it estimate background and ‘noise’ levels automatically. Note that our maps are in principle noise-free, so what is interpreted as noise in this procedure effectively arises from limitations due to source confusion, which leads to non-detections of some of the faintest and smallest sources. In a typical analysis with SExtractor, we resolve slightly more than half of the total SZ signal into discrete sources.

We measure the strength of a source as the monochromatic brightness change

$$S_\nu = \int_\Omega \Delta B_\nu d\Omega = f(x) B_\nu \int_\Omega y(\theta) d\Omega \quad (7)$$

of the CMB integrated over the solid angle of the source. Here B_ν is the Planck spectrum of the primary CMB, and $f(x)$ is the spectral function

$$f(x) = x \frac{e^x}{e^x - 1} \left(x \frac{e^x + 1}{e^x - 1} - 4 \right), \quad (8)$$

with $x = h\nu/kT_{\text{CMB}}$. In the following, we quote results for a frequency of 150 GHz.

In Fig. 7, we show the cumulative source counts per square degree found in the simulations 134A and 67A. We find remarkably good agreement between the two simulations, which differ by a factor of 8 in mass resolution. However, the higher resolution run 67A resolves a slightly larger number of faint (small) sources, while the bigger box 134A shows a small increase of the counts at the bright (large) end of the distribution. Both of these weak trends reflect expected effects due to box size and numerical resolution. Notice that the source counts we find are quite close to predictions by De Luca et al. (1995) based on Press-Schechter theory, however our simulations don’t show their exact power-law behavior at source strengths above 1 mJy. The dashed line in Fig. 7 gives the counts for the simulation with 1 keV energy injection. Interestingly, the counts for the bright sources are unaffected, but sources below a flux of 1 mJy (size of $\sim 30''$) are strongly reduced in number density, and still fainter (smaller) ones are practically eliminated.

Finally, we plot in Fig. 8 the differential flux distribution as a function of source strength. It is seen that the bulk of the total flux is provided by sources around 1 mJy, while the contribution by very faint and very bright sources is negligible. The good agreement at the faint end between the two adiabatic runs suggests that both of these simulations already resolve all the relevant sources that contribute significantly to the total Comptonization. Consistent with the results for the source counts, the energy injection run shows a strong suppression of faint SZ sources, while the brightest sources are nearly unaffected.

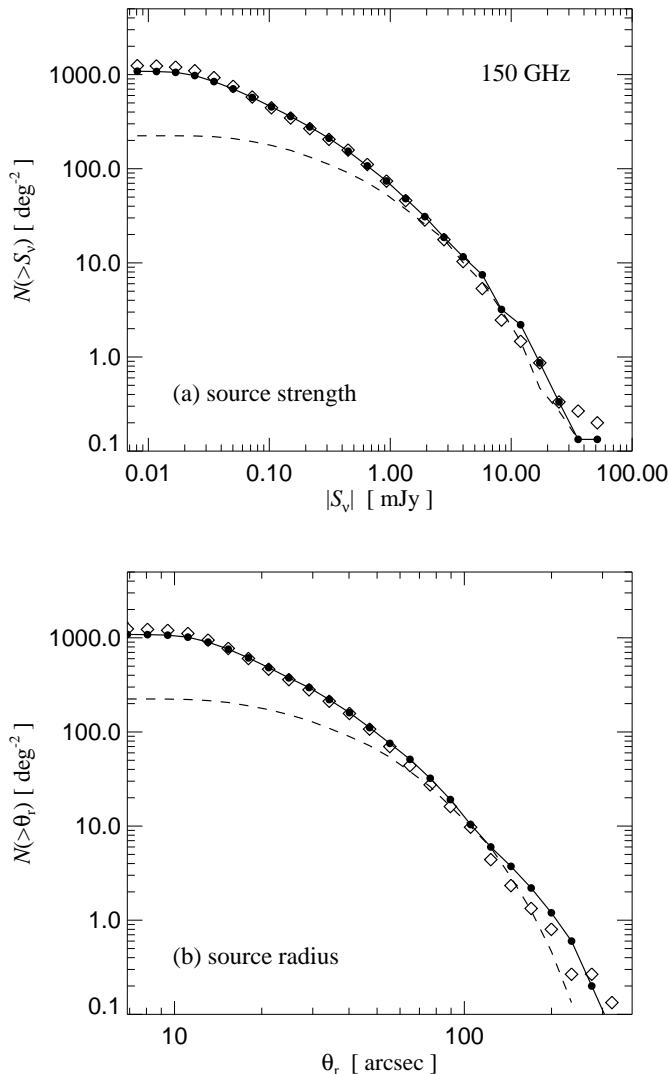


FIG. 7.— Cumulative counts of thermal SZ sources per square degree for models 134A (filled circles) and 67A (diamonds): (a) as a function of source strength, and (b) as a function of source radius. For each source, the source strength S_ν was defined as the integrated monochromatic flux decrement, integrated over the solid angle of the source. The radius of a source was computed based on the area detected by the source extraction software. In both panels, the dashed line shows the counts for the run with an injection of 1 keV of energy at $z = 7$.

4. DISCUSSION

We have performed a sequence of high resolution hydrodynamic simulations of structure formation in a Λ CDM model to investigate the thermal and kinetic Sunyaev-Zel'dovich effects. Figs. 1, 3, 7, and 8 show that including only adiabatic gas physics our simulations of the thermal effect are converged down to sub-arcminute scales. In particular, our results are well converged at the peak of the power spectrum, and they predict a mean Comptonization of $\langle y \rangle = 2.6 \times 10^{-6}$ for the adopted cosmology.

The detection of the brightest SZ sources with a density of ~ 1 per square degree requires an angular resolution of $\sim 1'$, and the capability to separate brightness fluctuations of size ~ 10 mJy (for 150 GHz) from the primary CMB fluctuations. Several current experiments are capable of meet-

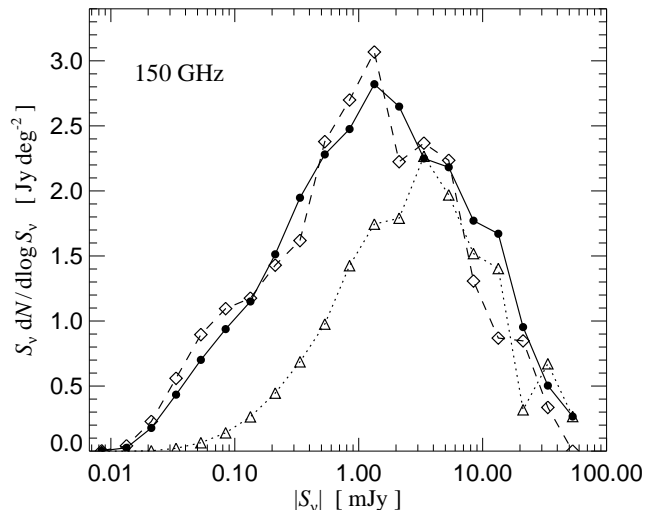


FIG. 8.— Differential flux distribution as a function of source strength for models 134A (filled circles) and 67A (diamonds). For each source, a source strength S_ν was defined as the integrated monochromatic flux decrement, integrated over the solid angle of the source. Triangles shows flux distribution for the run with an injection of 1 keV of energy at $z = 7$.

ing such requirements, for example the OVRO and BIMA interferometers, and they are already being used to detect and study SZ clusters. Improvements to these experiments should soon reduce the upper bounds shown in Fig. 3 and make the thermal SZ signal we predict detectable in the near future. The planned satellite mission *Planck Surveyor* with its high sensitivity and multi-frequency capability should allow a clean separation of the thermal SZ signal from the primary anisotropies, even though its angular resolution will be limited to less than $\ell \sim 1000$. However, future interferometric missions at mm-wavelengths, like ALMA, will be able to probe much smaller angular scales, up to $\ell \sim 10^6$, and should have enough sensitivity to detect both the thermal and kinetic effects. More detailed discussions of the prospects for extracting the SZ signal from upcoming CMB experiments are given elsewhere (Cooray, Hu & Tegmark 2000, Holder & Carlstrom 1999, and Bartlett 2000, among others).

We have examined the dependence of the SZ signal on early energy injection using an “extreme” model where 0.1 keV to 1 keV of energy was added into all of the gas at $z = 7$. The energy injection heats the gas, but also drives it out of small halos, erasing small-scale structure. The loss of small scale structures causes a reduction of the angular power spectrum at high- ℓ while the heating of the gas enhances the large angle signal (see Fig. 5).

In the runs without energy injection, most of the mean Comptonization is generated at redshifts $z \leq 3$, with a small tail extending to a redshift of about 5 (da Silva et al. 2000). However, in the runs with energy injection, additional Comptonization is provided by hot ionized gas in the IGM at still higher redshift. Current FIRAS limits on the mean Comptonization already exclude our most extreme model that injected 1 keV at $z = 7$. In future work, we will investigate the dependence of the SZ effects on additional input physics such as radiative cooling, star formation and its associated energy input by supernova

feedback.

We would like to acknowledge useful conversations with Rupert Croft, Chris Metzler, and Bill Holzapfel. This work was supported by NASA Astrophysical Theory Grant NAG5-3820 and by the NSF under grants ASC93-18185, ACI96-19019, and AST-9802568. M.W. was supported by NSF-9802362 and a Sloan Fellowship. The simulations were performed at the San Diego Supercomputer Center.

REFERENCES

- Bartlett J., 2000, preprint [astro-ph/0001267]
 Benson A.J., Nusser A., Sugiyama N., Lacey C.G., 2000, preprint [astro-ph/0002457]
 Bertin E., Arnouts S., 1996, *A&AS*, 117, 393
 Birkinshaw M., 1999, *Phys. Rep.*, 310, 98
 Bruscoli M., Ferrara A., Fabbri R., Ciardi B., 1999, preprint [astro-ph/9911467]
 Cavaliere A., Menci N., Tozzi P., 1998, *ApJ*, 501, 493
 Church S.E., Ganga K.M., Ade P.A.R., Holzapfel W.L., Mauskopf P.D., Wilbanks T.M., Lange A.E., 1997, *ApJ*, 484, 523
 Cooray A., 2000, preprint [astro-ph/0005287]
 Cooray A., Hu W., Tegmark M., 2000, preprint [astro-ph/0002238]
 Diaferio A., Sunyaev R.A., Nusser A., 2000, *ApJ*, 533, L71
 Fixsen D.J., Cheng E.S., Gales J.M., Mather J.C., Shafer R.A., Wright E.L., 1996, *ApJ*, 473, 576
 Gruzinov A., Hu W., 1998, *ApJ*, 508, 435
 De Luca A., Désert F.X., Puget J.L., 1995, *A&A*, 300, 335
 Hernquist L., Katz N., 1989, *ApJS*, 70, 419
 Holder G.P., Carlstrom J.E., 1999, in *Microwave Foregrounds*, ed. de Oliveira-Costa A. and Tegmark M., p.199, ASP Conference Series, San Francisco
 Holzapfel W.L., Carlstrom J.E., Grego L., Holder G., Joy M., Reese E.D., 2000, *ApJ*, 539, 57
 Hu W., White M., 1996, *A&A*, 315, 33
 Jones M.E., *Proceedings of the XVIth Moriond Astrophysics Meeting*, 1997, Edited by Bouchet F.R., Gispert R., Guilderdoni B., Jean Tran Thanh Van, p.161, Editions Frontieres
 Komastu E., Kitayama T., 1999, *ApJ*, 526, L1
 Molnar S.M., Birkinshaw M., 2000, *ApJ*, 537, 542
 Ostriker J., Steinhart P.J., 1995, *Nature*, 377, 600
 Ostriker J.P., Vishniac E.T., 1986, *ApJ*, 306, L51
 Partridge R.B., Richards E.A., Fomalont E.B., Kellerman K.I., Windhorst R.A., 1997, *ApJ*, 483, 38
 Pen U.-L., 1998, *ApJS*, 498, 60
 Pen U.-L., 1999, *ApJ*, 510, L1
 Persi F., Spergel D.N., Cen R., Ostriker J.P., 1995, *ApJ*, 442, 1
 Refregier A., Komatsu E., Spergel D.N., Pen U.-L., 2000, *Phys. Rev. D*, 61, 123001
 Rephaeli Y., 1995, *ARA&A*, 33, 541
 Seljak U., Burwell J., Pen U.-L., 2000, preprint [astro-ph/0001120]
 da Silva A.C., Barbosa D., Liddle A.R., Thomas P.A., 2000, preprint [astro-ph/9907224]
 Springel V., Yoshida N., White S.D.M., 2000, preprint [astro-ph/0003162]
 Subrahmanyam R., Ekers R.D., Sinclair M., Silk J., 1993, *MNRAS*, 263, 416
 Subrahmanyam R., Kesteven M.J., Ekers R.D., Sinclair M., Silk J., 1998, *MNRAS*, 298, 1189
 Sunyaev R.A., Zel'dovich Ya. B., 1972, *Comm. Astrophys. Space Phys.*, 4, 173
 Sunyaev R.A., Zel'dovich Ya. B., 1980, *ARA&A*, 18, 537
 Valageas P., Balbi A., Silk J., 2000, preprint [astro-ph/0009040]
 White M., Hu W., 2000, *ApJ*, 537, 1
 Wu K.K.S., Fabian A., Nulsen P.E.J., 1998, *MNRAS*, 301, L20
 Zhang P., Pen U.-L., 2000, preprint [astro-ph/0007462]